



This discussion paper is/has been under review for the journal Geoscientific Model Development (GMD). Please refer to the corresponding final paper in GMD if available.

The implementation of a MiXed Layer model (MXL, v1.0) for the dynamics of the atmospheric boundary layer in the Modular Earth Submodel System (MESSy)

R. H. H. Janssen and A. Pozzer

Atmospheric Chemistry Department, Max Planck Institute for Chemistry, Mainz, Germany

Received: 8 September 2014 – Accepted: 6 October 2014 – Published: 28 October 2014

Correspondence to: R. H. H. Janssen (ruud.janssen@mpic.de)

Published by Copernicus Publications on behalf of the European Geosciences Union.

GMDD

7, 7197–7238, 2014

Boundary layer dynamics with MXL/MESSy

R. H. H. Janssen and
A. Pozzer

Title Page

Abstract

Introduction

Conclusions

References

Tables

Figures



Back

Close

Full Screen / Esc

Printer-friendly Version

Interactive Discussion



Abstract

We present a new submodel for the Modular Earth Submodel System (MESSy): the MiXed Layer (MXL) model for the diurnal dynamics of the convective boundary layer, including explicit representations of entrainment and surface fluxes. Through the MESSy interface, MXL is coupled with modules that represent other processes relevant to chemistry in the atmospheric boundary layer (ABL). In combination, these provide a computationally inexpensive tool that is ideally suited for the analysis of field data, for evaluating new parametrizations for 3-D models, and for performing systematic sensitivity analyses. A case study for the DOMINO campaign in Southern Spain is shown to demonstrate the use and performance of MXL/MESSy in reproducing and analysing field observations.

1 Introduction

In atmospheric chemistry, various types of models are used for studies on different spatio-temporal scales, ranging from box models representing a single point in space (e.g. Sander et al., 2011) to regional and global 3-D models (e.g. Jöckel et al., 2006). Here, we describe the implementation of a MiXed Layer (MXL) submodel for the dynamics of the atmospheric boundary layer (ABL) in the Modular Earth Submodel System (MESSy, Jöckel et al., 2010). MXL represents the dynamics of the convective boundary layer at diurnal time-scales with two vertically changing layers, one for the ABL and one for the free troposphere (FT). In combination with MESSy submodels that represent the other processes relevant to atmospheric chemistry, it provides a missing link between box and 3-D atmospheric chemistry models, at a spatio-temporal scale typical for measurements of atmospheric chemistry. It is especially suited for studying the diurnal evolution of chemical species that have chemical lifetimes similar to the time scales of atmospheric mixing, so for which the effects of chemistry and dynamics should be studied simultaneously (Fig. 1). Since the typical time-scale of mixing of

GMDD

7, 7197–7238, 2014

Boundary layer dynamics with MXL/MESSy

R. H. H. Janssen and
A. Pozzer

Title Page

Abstract

Introduction

Conclusions

References

Tables

Figures



Back

Close

Full Screen / Esc

Printer-friendly Version

Interactive Discussion



a convective boundary layer is about 15 min., the evolution of species with a chemical time scale of minutes to several hours (e.g. O₃, isoprene, NO, and NO₂) will be to a similar extent driven by both dynamics and chemistry.

The MXL model has been developed in the 1960's and 1970's (Lilly, 1968; Tennekes, 1973) to study the dynamics of clear and cloudy boundary layers and was first applied to atmospheric chemistry by Vilà-Guerau de Arellano et al. (2009), as MXLCH (MXL-CHemistry). Afterwards MXLCH has been applied in studies of the diurnal evolution of gas-phase chemistry (Vilà-Guerau de Arellano et al., 2011; Ouwersloot et al., 2012; Van Stratum et al., 2012) and organic aerosol (Janssen et al., 2012, 2013) in mid-latitude, tropical and boreal areas. The model explicitly accounts for entrainment (ABL-FT exchange) and parametrizes turbulence in a simplified way. Although MXL uses simple parametrizations for turbulence and entrainment, the ABL dynamics as simulated by the model compare well with results from a turbulence resolving Large Eddy Simulation model (Pino et al., 2006) and with vertical profiles as observed from radio soundings (Ouwersloot et al., 2012).

With the implementation of MXL in MESSy (henceforth MXL/MESSy) as dynamical core and the subsequent coupling to the submodels that represent the other processes relevant to the evolution of chemical species in the troposphere, a versatile boundary layer chemistry model is created. MXL/MESSy can be used for different types of studies. First, it is well-suited to support the interpretation of field observations in an eulerian framework, e.g. observations from a tower. After obtaining a best fit with the observational data, a budget analysis can be performed, dividing the total tendency of species into the contributions of gas-phase chemistry, ABL dynamics, emission, deposition and/or gas/particle partitioning. The chemistry term can be further subdivided into the total production and loss terms, and the contributions of individual reactions to these terms.

Secondly, MXL/MESSy is well suited for performing systematic sensitivity analyses, in which the parameter space is explored and through which non-linearities can be studied. Because it is computationally inexpensive, detailed and systematic sensitivity

Boundary layer dynamics with MXL/MESSy

R. H. H. Janssen and
A. Pozzer

[Title Page](#)[Abstract](#)[Introduction](#)[Conclusions](#)[References](#)[Tables](#)[Figures](#)[Back](#)[Close](#)[Full Screen / Esc](#)[Printer-friendly Version](#)[Interactive Discussion](#)

runs are possible. In that way, it can serve as a test bed for new parametrizations, especially in combination with a direct comparison to field data. It thus forms a link between theoretical/lab study results and 3-D model applications. Finally, it can be used in theoretical/conceptual studies, for a qualitative evaluation of feedbacks and forcings (e.g. Vilà-Guerau de Arellano et al., 2012; Janssen et al., 2012).

In Sect. 2 we describe the MXL model and give its governing equations, in Sect. 3 we focus on the implementation of the MXL model in MESSy and in Sect. 4 we show an example application of MXL/MESSy using observations from the DOMINO campaign.

2 MXL submodel description

The version of the MiXed Layer model that we implement here has been developed in several stages: Lilly (1968) developed the mixed-layer equations and Tennekes (1973) the turbulence closure that we apply in this work. The model for the dynamics of the convective boundary layer that resulted from this work was later coupled to an atmospheric chemistry module by Vilà-Guerau de Arellano et al. (2009) and a land surface scheme by Van Heerwaarden et al. (2009, 2010).

The mixed layer theory states that under convective conditions, strong turbulent flow, driven by the surface heat fluxes, causes perfect mixing of quantities over the entire depth of the ABL (Vilà-Guerau de Arellano et al., 2015). Therefore, scalars and reactants in the convective boundary layer are characterized by well-mixed vertical profile over the whole depth of the ABL. The transition between the well-mixed ABL and the free troposphere is marked by an infinitesimally thin inversion layer. Typical profiles of potential temperature (θ), specific humidity (q) and chemical species in the mixed-layer model are shown in Fig. 2. It shows that the ABL is represented by bulk values of scalars and chemical species mixing ratios, and capped by a infinitesimally thin layer over which these strongly change. Above this inversion layer lies the residual layer (the remainder of the convective boundary layer of the previous day) during the early morning and the free troposphere later during the day, which are characterized in the model

Boundary layer dynamics with MXL/MESSy

R. H. H. Janssen and
A. Pozzer

Title Page

Abstract

Introduction

Conclusions

References

Tables

Figures

⏪

⏩

◀

▶

Back

Close

Full Screen / Esc

Printer-friendly Version

Interactive Discussion



by a lapse rate for heat and moisture, and a concentration profile of chemical species which is constant with height.

In addition to the local surface heat fluxes, the boundary layer dynamics can be influenced by large-scale atmospheric flows which act as external forcings on the ABL development: for instance, Janssen et al. (2013) and Pietersen et al. (2014) studied cases for which the observed ABL dynamics could only be reproduced if the influence of advection, caused by meso-scale flows, and/or subsidence, caused by a high-pressure system, were taken into account. Therefore, advection and subsidence can be prescribed as forcings to MXL.

2.1 Governing equations for the heat budget

The main variable in the dynamics of the convective boundary layer is the potential temperature (θ), since it is used to quantify the convective turbulence. The evolution of the potential temperature of a dry convective boundary layer is driven by the heat input at the surface (surface heat flux), at boundary layer top (entrainment heat flux) and at the lateral boundaries (advection):

$$\frac{\partial \langle \theta \rangle}{\partial t} = \frac{\overbrace{(w' \theta')_s}^{\text{surface heat flux}}}{h} - \frac{\overbrace{(w' \theta')_e}^{\text{entrainment heat flux}}}{h} + \underbrace{\text{adv}_\theta}_{\text{heat advection}} \quad (1)$$

Equation (1) is the result of a vertical integration of the 1-dimensional equation of the heat budget and we have assumed that the vertical profile of θ is in quasi-steady state (Lilly, 1968), which causes a linear vertical gradient of the heat flux. In this equation, $\overline{w' \theta'}_s$ is the kinematic heat flux at the surface, which is related to the sensible heat flux (SH) as: $\overline{w' \theta'}_s = \text{SH}/(\rho \cdot c_p)$, with ρ the density of air and c_p the specific heat of air. The entrainment process, represented by $\overline{(w' \theta')}_e$, is defined as the process whereby air from the FT is mixed in into the mixed layer, and it is therefore related to the θ jump

at the inversion. The evolution of $\langle \theta \rangle$ thus equals the input of heat into the ABL at the surface and due to entrainment over the ABL height h . Additionally, a heat advection term (adv_θ), which is a large-scale forcing on the boundary layer dynamics, can be prescribed to the model.

When calculating the entrainment flux, we assume that the transition from the ABL to the FT, the inversion, is represented by a sharp discontinuity, namely the zero-order jump closure (ZOJ, Tennekes, 1973). ZOJ closure defines this jump as $\Delta\theta = \theta_{\text{FT}} - \langle \theta \rangle$ over an infinitely thin inversion layer. In this ZOJ approach, the entrainment flux is the product of the entrainment velocity w_e (defined positive in the upward direction) and the potential temperature jump $\Delta\theta$ at the inversion. First-order closure approaches exist, which include the explicit representation of the depth of the entrainment zone, but the ZOJ approach already gives satisfactory results (Pino et al., 2006).

The equation for the potential temperature entrainment flux reads:

$$\left(\overline{w'\theta'}\right)_e = - \left(\frac{\partial h}{\partial t} - w_s\right) \Delta\theta = -w_e \cdot \Delta\theta \quad (2)$$

In our model, we calculate the subsidence velocity as:

$$w_s = -\omega h \quad (3)$$

where ω represents the large scale vertical velocity that is a function of the horizontal wind divergence in s^{-1} , i.e. $\omega = -\text{Div}(\mathbf{U})$; where \mathbf{U} is the horizontal wind. It can be thought of as the fraction with which the ABL is pushed down per second, due to large-scale subsiding air motions. Therefore, w_s is per definition negative.

By rewriting Eq. (2), we obtain an expression for the boundary layer growth $\left(\frac{\partial h}{\partial t}\right)$ as a function of the entrainment flux $\left(\overline{w'\theta'}\right)_e$, the potential temperature jump ($\Delta\theta$) and the subsidence velocity (w_s). It reads:

$$\frac{\partial h}{\partial t} = - \frac{\left(\overline{w'\theta'}\right)_e}{\Delta\theta} + w_s = w_e + w_s \quad (4)$$

In our model, we assume a value of β equal to 0.2, which physically means that the contribution of entrainment to the heat budget equals 20% of the contribution of the surface heat flux. The potential temperature is normally underestimated if this contribution is neglected. As we will show later on when introducing the moisture budget, Eq. (6) needs to be modified to make entrainment dependent on the buoyancy flux.

2.2 Governing equations for the moisture budget

By adding the moisture budget to the heat budget, we incorporate the effect of moisture on the buoyancy of air parcels and therewith complete the configuration of the thermodynamic variables in the ABL. The inclusion of the moisture effects on the dynamics of the ABL requires the introduction of two new equations. The first one (similar to Eq. 1) is the evolution of the mixed-layer specific humidity $\langle q \rangle$:

$$\frac{\partial \langle q \rangle}{\partial t} = \frac{\overbrace{(\overline{w'q'})_s}^{\text{surface moisture flux}}}{h} - \frac{\overbrace{(\overline{w'q'})_e}^{\text{entrainment moisture flux}}}{h} + \underbrace{\text{adv}_q}_{\text{moisture advection}} \quad (7)$$

where $\overbrace{(\overline{w'q'})_s}^{\text{surface moisture flux}}$ represents the surface specific moisture flux, $\overbrace{(\overline{w'q'})_e}^{\text{entrainment moisture flux}}$ the entrainment flux of moisture and adv_q an optionally prescribed moisture advection term. The specific moisture flux is related to the latent heat flux (LE) following $\overbrace{(\overline{w'q'})_s}^{\text{surface moisture flux}} = \text{LE}/(\rho \cdot L_v)$, with L_v the latent heat of vaporization. Similarly to Eq. (2), we represent the entrainment flux as:

$$\overbrace{(\overline{w'q'})_e}^{\text{entrainment moisture flux}} = - \left(\frac{\partial h}{\partial t} - w_s \right) \Delta q = -w_e \cdot \Delta q. \quad (8)$$

This equation relates the dynamics of the boundary layer growth, represented by the entrainment velocity, with the specific humidity jump at the interface between the ABL and the FT.

Equation (8) requires an additional equation for the temporal evolution of the jump of q at the ABL-FT interface (Δq). It reads:

$$\frac{\partial \Delta q}{\partial t} = \frac{\partial q_{\text{FT}}}{\partial t} - \frac{\partial \langle q \rangle}{\partial t} = \gamma_q \left(\frac{\partial h}{\partial t} - w_s \right) - \frac{\partial \langle q \rangle}{\partial t} \quad (9)$$

where γ_q is the lapse rate of q in the FT.

At this point, we need to introduce a new variable, the virtual potential temperature, which accounts for the both changes in the heat and moisture budgets and is used to quantify buoyancy. It is defined as:

$$\theta_v = \theta(1 + 0.61q) \quad (10)$$

The virtual potential temperature thus account for the effect of water vapour on the density of air. Since moist air is less dense than dry air at the same conditions of temperature and pressure, θ_v is always greater than the actual temperature, but only by a few degrees. The turbulent transport of this variable, the buoyancy flux, combines in one quantity the information of the potential temperature flux and the specific moisture flux. It reads:

$$\overline{w'\theta'_v} = \overline{w'\theta'} + 0.61 \left(\langle \theta \rangle \overline{w'q'} + \langle q \rangle \overline{w'\theta'} + \overline{w'\theta'q'} \right) \approx \overline{w'\theta'} + 0.61 \left(\langle \theta \rangle \overline{w'q'} \right). \quad (11)$$

This buoyancy flux expresses the production of turbulent kinetic energy in the ABL due to density differences. Turbulence driven by shear (mechanical turbulence) on the mixed-layer thermodynamic equations is not dealt with in our model.

The buoyancy flux directly enters in the ABL growth formulated in Eq. (2). Therefore, we rewrite Eq. (2) in the definitive form as:

$$\left(\overline{w'\theta'_v} \right)_e = - \left(\frac{\partial h}{\partial t} - w_s \right) \Delta \theta_v = -w_e \cdot \Delta \theta_v, \quad (12)$$

where $\Delta \theta_v$ is expressed in terms of the characteristics of the θ - and q -budgets:

$$\Delta \theta_v = \Delta \theta + 0.61 \left(\langle q \rangle \Delta \theta + \langle \theta \rangle \Delta q + \Delta \theta \Delta q \right) \quad (13)$$

By introducing the buoyancy flux as the driver of the turbulent process in the determination of the boundary layer growth, we complete the main framework of our model formulation based on mixed-layer theory.

In summary, the combined heat and moisture system is composed by the following 6 equations:

1. prognostic budget equations for $\langle\theta\rangle$ and $\langle q\rangle$ (Eqs. 1 and 7),
2. boundary layer growth (Eq. 12) rewritten as:

$$\frac{\partial h}{\partial t} = -\frac{\overline{(w'\theta'_v)}_e}{\Delta\theta_v} + w_s, \quad (14)$$

3. prognostic equations for $\Delta\theta$ and Δq (Eqs. 5 and 9),
4. closure assumption relating the surface buoyancy flux to the entrainment buoyancy flux $\overline{(w'\theta'_v)}_e = -\beta \overline{(w'\theta'_v)}_s$.

2.3 Governing equations for the horizontal wind budget

As the last part of the mixed-layer dynamics, we introduce the horizontal wind, or the momentum budget. The wind speed is important for calculating surface-atmosphere exchange, and appears for instance in the calculations of the aerodynamic resistance which governs evapotranspiration (Sect. 2.7.2) and dry deposition.

Similar expressions as for $\langle\theta\rangle$ and $\langle q\rangle$ can be used for the two horizontal components of the wind speed. These equations also contain the Coriolis force that takes into

Boundary layer dynamics with MXL/MESSy

R. H. H. Janssen and
A. Pozzer

Title Page

Abstract

Introduction

Conclusions

References

Tables

Figures



Back

Close

Full Screen / Esc

Printer-friendly Version

Interactive Discussion



account the rotation of the Earth. This gives another four equations:

$$\frac{d\langle u \rangle}{dt} = \frac{(\overline{u'w'})_s}{h} + \frac{(\overline{u'w'})_e}{h} - f_c \Delta v \quad (15)$$

$$\frac{d\langle v \rangle}{dt} = \frac{(\overline{v'w'})_s}{h} + \frac{(\overline{v'w'})_e}{h} + f_c \Delta u \quad (16)$$

$$\frac{d\Delta u}{dt} = \gamma_u w_e - \frac{d\langle u \rangle}{dt} \quad (17)$$

$$\frac{d\Delta v}{dt} = \gamma_v w_e - \frac{d\langle v \rangle}{dt} \quad (18)$$

where $\langle u \rangle$ and $\langle v \rangle$ are the mixed-layer wind velocities in x and y direction, Δu and Δv are the jumps of these two variables, γ_u and γ_v are the lapse rates in the FT and f_c is the Coriolis parameter. The free tropospheric wind velocities are assumed to be equal to the geostrophic wind at their height. Also for the wind budget, we assume zero-order closure:

$$\overline{(u'w')_e} = -w_e \cdot \Delta u \quad (19)$$

$$\overline{(v'w')_e} = -w_e \cdot \Delta v \quad (20)$$

For applications such as in Eq. (41), u and v are combined to form the total horizontal wind speed:

$$U = \sqrt{\langle u^2 \rangle + \langle v^2 \rangle + w_*^2} \quad (21)$$

where w_* is the free convection scaling velocity:

$$w_* = \left(\frac{g \cdot h}{\theta_v} \overline{w' \theta'_{v,s}} \right)^{1/3} \quad (22)$$

Boundary layer dynamics with MXL/MESSy

R. H. H. Janssen and A. Pozzer

Title Page

Abstract

Introduction

Conclusions

References

Tables

Figures

◀

▶

◀

▶

Back

Close

Full Screen / Esc

Printer-friendly Version

Interactive Discussion



2.4 Governing equations for chemical species

The mixed-layer model allows us to investigate the influence of the boundary layer dynamics on reactive atmospheric compounds during daytime. It is important to stress that in mixed-layer theory, we assume that species are mixed instantaneously as soon as they are chemically produced, emitted or entrained from the FT. In other words, the MXL model acts as a reactive chamber with the additional advantage of accounting for boundary layer growth and ABL-FT exchange.

As for scalars, the inclusion of reactive species requires the introduction of two additional equations for each species. The expression for the evolution of the generic species C is similar to that for potential temperature (Eq. 1) and moisture (Eq. 7), but includes a term for the chemical transformation:

$$\frac{\partial \langle C \rangle}{\partial t} = \frac{\overbrace{(\overline{w' C'})_s}^{\text{emis./dep. flux}}}{h} - \frac{\overbrace{(\overline{w' C'})_e}^{\text{entrainment flux}}}{h} + \underbrace{S_C}_{\text{chemistry}} \quad (23)$$

By solving Eq. (23), we determine how C varies over time as a function of emission/deposition processes at the surface (represented by the term $(\overline{w' C'})_s$), the dynamic effects (h and $(\overline{w' C'})_e$) and the chemical transformation (S_C). Note that the surface fluxes of chemical species (emission or deposition) can be either prescribed (Sect. 2.5) to MXL/MESSy or calculated by other MESSy submodels (Sect. 3.1, Table 1). Advection of tracers is not considered, because horizontal gradients in species concentrations, which are necessary to calculate advection, are generally not constrained by observations. We are planning to implement the TNUDGE submodel (Kerkweg et al., 2006b) in the future to allow the relaxation of chemical species concentrations towards observations, which will also compensate for sources or sinks that are the result of advection of air masses with different concentrations of species.

Boundary layer dynamics with MXL/MESSy

R. H. H. Janssen and
A. Pozzer

Title Page

Abstract

Introduction

Conclusions

References

Tables

Figures

◀

▶

◀

▶

Back

Close

Full Screen / Esc

Printer-friendly Version

Interactive Discussion



The flux at the top of the boundary layer is represented in the same way as the entrainment flux for buoyancy, moisture and wind. For C it reads:

$$\left(\overline{w'C'}\right)_e = -w_e \cdot \Delta C \quad (24)$$

By representing the exchange of C as the product of the entrainment velocity and the jump of C , we account for both the dynamics and chemistry, which together determine the exchange between the ABL and FT.

Equation (24) requires an additional prognostic equation to solve the evolution of ΔC :

$$\frac{\partial \Delta C}{\partial t} = \frac{\partial C_{FT}}{\partial t} - \frac{\partial \langle C \rangle}{\partial t} \quad (25)$$

where C_{FT} is the concentration of C in the FT with $\partial C_{FT} / \partial t$ driven by chemical production and loss only in MXL/MESSy.

By assuming instantaneous mixing, we assume that the intensity of segregation of chemical species due to possible inefficient turbulent mixing is zero. It has been hypothesized that this segregation might be important for explaining model-measurements discrepancies for certain species, e.g. isoprene and the hydroxyl radical (Butler et al., 2008; Pugh et al., 2010). Later studies, however, showed that the effects of imperfect mixing are only small, with a maximum reduction of the effective rate constant for the isoprene and OH by less than 15 % (Ouwensloot et al., 2011; Pugh et al., 2011), and not by as much as 50 %, which was necessary to explain the measurement-model discrepancy. Moreover, Large Eddy Simulation results show well-mixed profiles throughout the convective boundary layer for species like isoprene and OH (Vilà-Guerau de Arellano et al., 2009, 2011; Ouwensloot et al., 2011) under homogeneous land surface conditions. A parametrization for the effect of the segregation of species on the effective rate constants was developed by Vinuesa and Vilà-Guerau de Arellano (2003) and can in principle be implemented to account for this effect.

Boundary layer dynamics with MXL/MESSy

R. H. H. Janssen and A. Pozzer

Title Page

Abstract

Introduction

Conclusions

References

Tables

Figures

⏪

⏩

◀

▶

Back

Close

Full Screen / Esc

Printer-friendly Version

Interactive Discussion



Boundary layer dynamics with MXL/MESSy

R. H. H. Janssen and
A. Pozzer

Title Page

Abstract

Introduction

Conclusions

References

Tables

Figures

◀

▶

◀

▶

Back

Close

Full Screen / Esc

Printer-friendly Version

Interactive Discussion



The incoming short wave radiation S_{in} is calculated by:

$$S_{in} = S_0 T_r \sin(\Psi) \quad (30)$$

where S_0 is the constant solar irradiance at the top of the atmosphere, taken at 1365 W m^{-2} , T_r the net sky transmissivity, that takes into account the influence of radiative path length and atmospheric absorption and scattering using:

$$T_r = 0.6 + 0.2 \sin(\Psi) \quad (31)$$

Through Ψ , both expressions depend on geographical location, day of the year and time of the day. Ψ is calculated using:

$$\sin(\Psi) = \sin(\phi) \sin(\delta_s) - \cos(\phi) \cos(\delta_s) \cos\left(2\pi \frac{t_{UTC}}{t_d} + \lambda_e\right) \quad (32)$$

where t_{UTC} is the universal time (UTC) and t_d is the diurnal period of 24 h. The latitude ϕ (positive north of Equator) and longitude λ_e (positive east of Greenwich) define the geographic location. Variable δ_s is the solar declination, which is a function of the day number:

$$\delta_s = \Phi_r \cos\left(2\pi \frac{d - d_r}{d_y}\right) \quad (33)$$

where Φ_r is the tilt of the Earth's axis relative to the elliptic, equal to 0.409 rad. The Julian day is represented by d and d_r is 173. The number of days in a year d_y is taken as 365.

The outgoing shortwave radiation depends on the surface albedo:

$$S_{out} = \alpha S_{in} \quad (34)$$

where α is the surface albedo.

The outgoing long wave radiation is calculated using the the Stefan–Boltzmann Law:

$$L_{\text{out}} = \epsilon_s \sigma_{\text{SB}} T_s^4 \quad (35)$$

where ϵ_s is the surface emissivity taken equal to 1, σ_{SB} the Stefan–Boltzmann constant equal to $5.67 \times 10^{-8} \text{ W m}^{-2} \text{ K}^{-4}$, and T_s the surface temperature (K).

The incoming long wave radiation is computed using the same expression, but here it uses the temperature at the top of the surface layer T_{sl} . This temperature is acquired by converting the potential temperature of the mixed-layer θ to absolute temperature using the height of surface layer top, which we define as 10% of the boundary-layer height h . This gives the expression:

$$L_{\text{in}} = \epsilon_a \sigma_{\text{SB}} T_{\text{sl}}^4 \quad (36)$$

where the atmospheric emissivity ϵ_a is 0.8.

2.7 Land surface model

A land surface model (Van Heerwaarden et al., 2009, 2010; Van Heerwaarden, 2011) is included as an option in MXL/MESSy, which enables the interactive calculation of surface heat fluxes. With this inclusion, MXL/MESSy can be used to simultaneously and interactively calculate the exchange of energy (sensible heat flux), water (latent heat flux), wind (momentum flux) and chemical species (emission and deposition) between the land surface and the ABL. In that way, a fully online coupled land surface-ABL chemistry model is obtained, in which all exchanges between the land surface and the ABL at the diurnal time-scale are internal variables of the coupled system. This means that only forcings (drivers external to the system at the appropriate time scales) are prescribed to the model. These includes land surface forcings (e.g. leaf area index (LAI), roughness length, soil moisture) and large-scale meteorological forcings on the ABL (e.g. incoming solar radiation, FT conditions).

Title Page

Abstract

Introduction

Conclusions

References

Tables

Figures

⏪

⏩

◀

▶

Back

Close

Full Screen / Esc

Printer-friendly Version

Interactive Discussion



2.7.1 The surface energy balance

The surface energy balance (SEB) forms the basis for the land surface model. It relates net radiation R_n (Eq. 29) to the surface heat fluxes:

$$R_n - G = SH + LE \quad (37)$$

where SH is the sensible heat flux, LE is the latent heat flux and G is the ground heat flux.

The sensible and latent heat flux, which together supply the energy to the atmosphere that drives turbulent convection, are a function of land surface and atmospheric properties:

$$SH = \frac{\rho c_p}{r_a} (\theta_s - \langle \theta \rangle) \quad (38)$$

$$LE = \frac{\rho L_v}{r_a + r_s} (q_{\text{sat}}(T_s) - \langle q \rangle) \quad (39)$$

where r_a is the aerodynamic resistance, r_s is the surface resistance, θ_s and $\langle \theta \rangle$ are the potential temperatures of the surface and the mixed-layer respectively, $q_{\text{sat}}(T_s)$ is the saturated specific humidity inside the canopy and $\langle q \rangle$ is the mixed-layer specific humidity.

The Penman–Monteith equation (Monteith, 1965) is then used to relate the evaporation flux to radiation, temperature, humidity, and aerodynamic and surface resistance:

$$LE = \frac{\frac{dq_{\text{sat}}}{dT} (R_n - G) + \frac{\rho c_p}{r_a} (q_{\text{sat}}(T) - \langle q \rangle)}{\frac{dq_{\text{sat}}}{dT} + \frac{c_p}{L_v} \left(1 + \frac{r_s}{r_a} \right)}, \quad (40)$$

where $\frac{dq_{\text{sat}}}{dT}$, which is the slope of the saturated specific humidity curve with respect to temperature, and q_{sat} are evaluated using the atmospheric mixed-layer temperature at the top of the atmospheric surface layer defined as $z_{\text{sl}} = 0.1h$.

Boundary layer dynamics with MXL/MESSy

R. H. H. Janssen and
A. Pozzer

Title Page

Abstract

Introduction

Conclusions

References

Tables

Figures

◀

▶

◀

▶

Back

Close

Full Screen / Esc

Printer-friendly Version

Interactive Discussion



2.7.2 Resistances

The exchange of momentum and heat between the atmosphere with the surface is related to the strength of the turbulence. The aerodynamic resistance r_a , that appears in Eqs. (38) and (39) is the inverse of this turbulent intensity and defined as:

$$r_a = \frac{1}{C_H \langle U \rangle} \quad (41)$$

where C_H is the drag coefficient for heat and $\langle U \rangle$ is the mixed-layer wind speed (Sect. 2.3). It shows that stronger winds lead to lower aerodynamic resistance and enhanced turbulent exchange.

The turbulent exchange also depends on the drag, which is a function of the stability of the surface layer: a growing instability in the surface layer leads to stronger convection and mixing. The drag coefficient is calculated following:

$$C_H = \frac{\kappa^2}{A \cdot B} \quad (42)$$

with:

$$A = \ln \left(\frac{z_{sl}}{z_{0m}} \right) - \Psi_M \left(\frac{z_{sl}}{L} \right) + \Psi_M \left(\frac{z_{0m}}{L} \right)$$

$$B = \ln \left(\frac{z_{sl}}{z_{0h}} \right) - \Psi_H \left(\frac{z_{sl}}{L} \right) + \Psi_H \left(\frac{z_{0h}}{L} \right)$$

where κ is the von Kármán constant, z_{0m} and z_{0h} are the roughness lengths for momentum and heat, respectively, z_{sl} is the depth of the atmospheric surface layer of $0.1h$, L is the Monin–Obukhov length and Ψ_M and Ψ_H are the integrated stability functions for momentum and heat taken from Beljaars (1991). To find the values of L that are required in this function, the following implicit function is solved using a Newton–Raphson

Boundary layer dynamics with MXL/MESSy

R. H. H. Janssen and
A. Pozzer

Title Page

Abstract

Introduction

Conclusions

References

Tables

Figures

⏪

⏩

◀

▶

Back

Close

Full Screen / Esc

Printer-friendly Version

Interactive Discussion



iteration method:

$$\begin{aligned}
 Ri_B &= \frac{g}{\langle \theta_v \rangle} \frac{z_{sl} (\langle \theta_v \rangle - \theta_{vs})}{U^2} \\
 &= \frac{z_{sl}}{L} \frac{\left[\ln \left(\frac{z_{sl}}{z_{0h}} \right) - \Psi_H \left(\frac{z_{sl}}{L} \right) + \Psi_H \left(\frac{z_{0h}}{L} \right) \right]}{\left[\ln \left(\frac{z_{sl}}{z_{0m}} \right) - \Psi_M \left(\frac{z_{sl}}{L} \right) + \Psi_M \left(\frac{z_{0m}}{L} \right) \right]^2}
 \end{aligned} \tag{43}$$

5 where Ri_B is the bulk Richardson number and θ_{vs} and $\langle \theta_v \rangle$ are the virtual potential temperatures of the surface and the mixed-layer atmosphere respectively.

The calculations of both resistances r_{veg} and r_{soil} follow the method of Jarvis (1976) and employed similarly as in the ECMWF global forecasting model. The vegetation resistance is based on the following multiplicative equation.

$$10 \quad r_{veg} = \frac{r_{s, \min}}{LAI} f_1(S_{in}) f_2(w_{soil2}) f_3(VPD) f_4(T) \tag{44}$$

15 where $r_{s, \min}$ is the minimum surface resistance, LAI the leaf area index of the vegetated fraction, f_1 a correction function depending on incoming short wave radiation S_{in} , f_2 a function depending on soil moisture w , f_3 a function depending on vapor pressure deficit (VPD) and f_4 a function depending on temperature T . Of these correction functions, the first three originate from the ECMWF model documentation and the fourth from Noilhan and Planton (1989) and are defined as:

$$\frac{1}{f_1(S_{in})} = \min \left(1, \frac{0.004 S_{in} + 0.05}{0.81 (0.004 S_{in} + 1)} \right) \tag{45}$$

$$\frac{1}{f_2(w)} = \frac{w - w_{wilt}}{w_{fc} - w_{wilt}} \tag{46}$$

$$\frac{1}{f_3(VPD)} = \exp(g_D VPD) \tag{47}$$

$$\frac{1}{f_4(T)} = 1.0 - 0.0016(298.0 - T)^2, \quad (48)$$

where w_{wilt} is the volumetric soil moisture at wilting point, w_{fc} is the volumetric soil moisture at field capacity and g_D is a correction factor for vapor pressure deficit that only plays a role in high vegetation.

The soil resistance depends on the amount of soil moisture in the layer that has direct contact with the atmosphere.

$$r_{\text{soil}} = r_{s, \text{min}} f_2(w_{\text{soil}1}), \quad (49)$$

where f_2 is calculated following Eq. (46).

2.7.3 Evapotranspiration calculation

The total evapotranspiration consist of three parts: soil evaporation, leaf transpiration and evaporation of liquid water from the leaf surface. The total evapotranspiration is therefore proportional to the vegetated fraction of the land surface:

$$LE_{\text{tot}} = c_{\text{veg}}(1 - c_{\text{liq}})LE_{\text{veg}} + c_{\text{veg}}c_{\text{liq}}LE_{\text{liq}} + (1 - c_{\text{veg}})LE_{\text{soil}}, \quad (50)$$

where LE_{tot} is the evapotranspiration, LE_{veg} the transpiration from vegetation, LE_{soil} the evaporation from the soil and LE_{liq} evaporation of liquid water. The fractions that are used are c_{veg} which is the fraction of the total area that is covered by vegetation and c_{liq} , which is the fraction of the vegetated area that contains liquid water. Since c_{liq} is not constant in time, it is modeled following:

$$c_{\text{liq}} = \frac{W_l}{LAI W_{\text{max}}} \quad (51)$$

where W_{max} is the representative depth of a water layer that can lay on one leaf and W_l the actual water depth. The evolution of W_l is governed by the following equation:

$$\frac{dW_l}{dt} = \frac{LE_{\text{liq}}}{\rho_w L_v} \quad (52)$$

Boundary layer dynamics with MXL/MESSy

R. H. H. Janssen and A. Pozzer

Title Page	
Abstract	Introduction
Conclusions	References
Tables	Figures
◀	▶
◀	▶
Back	Close
Full Screen / Esc	
Printer-friendly Version	
Interactive Discussion	



3 Implementation in the MESSy structure

For the implementation of MXL, a generic 1-D basemodel is created in MESSy, called VERTICO (VERTICAL COLUMN), which defines the number of boxes stacked on top of each other and directs the time integration. VERTICO is a de facto 3-D model in which the horizontal resolution has been reduced to a single grid box, to facilitate the submodel coupling within the MESSy framework. This also facilitates the possible development of a column model that includes more vertical levels in both boundary layer and free troposphere.

The current implementation of VERTICO consists of two domains (see Fig. 4): the lower one represents the well-mixed boundary layer during daytime, as represented by the MXL equations, and the upper box contains a simplified description of the free troposphere on top of the ABL. The prognostic equations for the ABL dynamics and the land surface scheme are integrated by an Euler forward solver.

3.1 Coupling with other MESSy submodels

Through the MESSy framework, two types of submodels are coupled: the first type are the generic submodels, which constitute the model infrastructure that is not directly related to actual physical processes, such as time, tracer and data management. The second type are the process submodels, which represent the individual processes that contribute to the evolution of chemical species in the ABL (see Eq. 23 and Fig. 3). Table 1 shows all generic and process submodels that are currently coupled to form MXL/MESSy, and their tasks. In principle, thanks to such an implementation, any MESSy submodel can be used in MXL/MESSy.

The modular nature of the MESSy interface allows full flexibility: processes can easily be switched on and off through switches in a namelist. Emission and deposition of species takes place only in the lower box, while chemistry and gas/particle partitioning take place in both ABL and FT. The chemical production and loss of a species is calculated in the MECCA submodel (Sander et al., 2011), which uses photolysis rates

Boundary layer dynamics with MXL/MESSy

R. H. H. Janssen and
A. Pozzer

Title Page

Abstract

Introduction

Conclusions

References

Tables

Figures



Back

Close

Full Screen / Esc

Printer-friendly Version

Interactive Discussion



from JVAL (Sander et al., 2014). For the lower boundary conditions, there are two possibilities. On one hand, MXL/MESSy offers the possibility to use interactive emission (via the ONEMIS, Kerkweg et al., 2006b and MEGAN Guenther et al., 2006 submodels), dry deposition (DDEP Kerkweg et al., 2006a) and land surface parametrisations (Sect. 2.7). In these submodels, land surface-ABL exchange is calculated as function of land surface and ABL characteristics, like stomatal resistance and air temperature. On the other hand, it is possible to prescribe emissions and surface heat fluxes following simplified functions for the users who like to keep full control over the boundary conditions of the model (Sect. 2.5). In that way, MXL/MESSy can for instance be used to evaluate the sensitivity of the chemistry in the ABL to uncertainties in emission estimates. Further, OFFEMIS (Kerkweg et al., 2006b) allows for the extraction of emission data from an emission database. Additionally, the organic aerosol submodel ORACLE (Tsimpidi et al., 2014), allows for the representation of the organic aerosol composition and evolution.

4 DOMINO case study

To evaluate MXL/MESSy, we revisited the case study of Van Stratum et al. (2012), which is based on observations from the DOMINO campaign in the south of Spain. MXL/MESSy, with initial conditions as in Table A1, represents the dynamics of the boundary layer well, as compared to observations from a tower and radio soundings (Fig. 5). Since the equations and the initial and boundary conditions are equal to those of Van Stratum et al. (2012), the dynamics of $\langle\theta\rangle$, $\langle q\rangle$ and h are identical to those shown in their Fig. 3. As a result of the positive heat fluxes (Fig. 5d), the initial potential temperature inversion is broken after 09:00 LT, and the boundary layer starts to grow rapidly. During this period of strong ABL growth, air from the FT is entrained, which causes (1) a strong increase in the $\langle\theta\rangle$, since warm air from the FT is entrained and (2) a decrease in $\langle q\rangle$ despite the positive latent heat flux, since dry air from the FT is entrained into the ABL. After 13:00 LT, the ABL growth slows down, and the effect of entrainment

Boundary layer dynamics with MXL/MESSy

R. H. H. Janssen and
A. Pozzer

Title Page

Abstract

Introduction

Conclusions

References

Tables

Figures

⏪

⏩

◀

▶

Back

Close

Full Screen / Esc

Printer-friendly Version

Interactive Discussion



on scalars and chemical species becomes smaller. The correct representation of the boundary layer dynamics ensures that we also simulate the effect of ABL dynamics on the evolution of chemical species well (through h and w_e in Eqs. 23 and 24).

Figure 6 shows the diurnal evolution of several gas-phase chemical species, from measurements and from three model runs:

- the MXL/MESSy code with MIM2 chemistry (Taraborrelli et al., 2009), with initial conditions as in Van Stratum et al. (2012) (SameIC),
- the MXL/MESSy code with MIM2 chemistry (Taraborrelli et al., 2009), with initial conditions that gave the best fit with the measurements (BestFit),
- the MXLCH code as in Van Stratum et al. (2012).

The MESSy/MXL SameIC and MXLCH simulations were performed with identical initial conditions as listed in Table A2. In the MXL/MESSy SameIC run we overestimate NO, NO₂ and isoprene and underestimate O₃, HO₂ and H₂O₂. However, these results are influenced by the surface fluxes (emission and deposition) and the mixing ratios in the FT of several species. Since these were not measured, this gives us some degrees of freedom to adjust them, within realistic bounds, to obtain an improved fit of MXL/MESSy with the observations.

Figure 6 also shows the MXL/MESSy BestFit results (with initial conditions as in Table A2). It shows that MXL/MESSy with the MIM2 chemical mechanism is able to reproduce the diurnal dynamics of the main gas-phase chemical species well. While it reproduces the timing and peak values of OH and HO₂ well, the mixing ratios of both radicals are underestimated in the early morning and late afternoon. Also H₂O₂ is underestimated from 10.00 a.m. to the late afternoon, which is related to the underestimation of HO₂.

To give more insight in the diurnal evolution of chemical species, it is useful to analyse the contributions of the different processes to the total tendency (Eq. 23). The modular nature of MXL/MESSy facilitates the evaluation of the contributions of the individual processes, thanks to the diagnostic tools present in the MESSy framework.

Boundary layer dynamics with MXL/MESSy

R. H. H. Janssen and
A. Pozzer

[Title Page](#)[Abstract](#)[Introduction](#)[Conclusions](#)[References](#)[Tables](#)[Figures](#)[Back](#)[Close](#)[Full Screen / Esc](#)[Printer-friendly Version](#)[Interactive Discussion](#)

**Boundary layer
dynamics with
MXL/MESSy**R. H. H. Janssen and
A. Pozzer[Title Page](#)[Abstract](#)[Introduction](#)[Conclusions](#)[References](#)[Tables](#)[Figures](#)[⏪](#)[⏩](#)[◀](#)[▶](#)[Back](#)[Close](#)[Full Screen / Esc](#)[Printer-friendly Version](#)[Interactive Discussion](#)

In Fig. 7, an example is shown for O_3 , based on the optimally tuned (BestFit) simulation. The upper panel shows how the total O_3 tendency is built up from the contributions of chemistry, entrainment and dry deposition (although the latter is set to zero), and the lower panel shows the chemistry term and how gas-phase and photolysis reactions contribute to the loss and production of ozone in the ABL. The contribution of entrainment to the O_3 budget is strongest during the morning when the ABL grows rapidly and a large quantity of ozone-rich air is mixed in into the ABL from the FT. Except for the early morning and late afternoon, the sum of the chemical production and destruction of O_3 is positive, and the net O_3 production peaks around noon when photochemistry is strongest. Note that while we chose to show total production and loss terms for O_3 here, it is possible to split up these terms into the contributions of the individual reactions.

5 Summary

We have implemented the MXL model as a new submodel in MESSy, in order to represent the diurnal dynamics of the atmospheric boundary layer and their effect on atmospheric chemistry. The comprehensiveness of MXL/MESSy in representing the processes relevant to atmospheric chemistry in the convective boundary layer, while keeping computational requirements low, makes it an ideal tool for applications in atmospheric chemistry that ask for systematic sensitivity analyses. These include the interpretation of observations from field campaigns and the evaluation of new process parametrizations under ambient conditions, as well as theoretical studies on the coupled land surface-boundary layer-atmospheric chemistry system. Expansion of the model with additional relevant MESSy submodels and conversion into a multi-layer column model is planned for the future: e.g. including the surface layer, entrainment zone, account for imperfect mixing in ABL (e.g. due to clouds, aerosol layers) and the stable nocturnal boundary layer.

Code availability

MXL/MESSy is part of the Modular Earth Submodel System (MESSy), which is continuously further developed and applied by a consortium of institutions. The usage of MESSy and access to the source code is licenced to all affiliates of institutions which are members of the MESSy Consortium. Institutions can be a member of the MESSy Consortium by signing the MESSy Memorandum of Understanding. More information can be found on the MESSy Consortium Website (www.messy-interface.org).

The Supplement related to this article is available online at doi:10.5194/gmdd-7-7197-2014-supplement.

Acknowledgements. The authors thank Jordi Vilà for his useful comments on the DOMINO data and on the manuscript, Rolf Sander and Sergey Gromov for their helpful discussions on the implementation of MXL in MESSy and Chiel van Heerwaarden for providing the land surface scheme equations.

The service charges for this open access publication have been covered by the Max Planck Society.

References

- Beljaars, A. C. M.: Numerical Schemes for Parametrizations, ECMWF Seminar on Numerical Methods in Atmospheric Models, Reading, UK, 9–13 September 1991, 1–42, 1991. 7214
- Butler, T. M., Taraborrelli, D., Brühl, C., Fischer, H., Harder, H., Martinez, M., Williams, J., Lawrence, M. G., and Lelieveld, J.: Improved simulation of isoprene oxidation chemistry with the ECHAM5/MESSy chemistry–climate model: lessons from the GABRIEL airborne field campaign, *Atmos. Chem. Phys.*, 8, 4529–4546, doi:10.5194/acp-8-4529-2008, 2008. 7209
- Clapp, R. B. and Hornberger, G. M.: Empirical equations for some soil hydraulic properties, *Water Resour. Res.*, 14, 601–604, doi:10.1029/WR014i004p00601, 1978. 7217, 7218

Boundary layer dynamics with MXL/MESSy

R. H. H. Janssen and
A. Pozzer

Title Page

Abstract

Introduction

Conclusions

References

Tables

Figures



Back

Close

Full Screen / Esc

Printer-friendly Version

Interactive Discussion



Boundary layer dynamics with MXL/MESSy

R. H. H. Janssen and
A. Pozzer

Title Page

Abstract

Introduction

Conclusions

References

Tables

Figures



Back

Close

Full Screen / Esc

Printer-friendly Version

Interactive Discussion



Conzemius, R. J. and Fedorovich, E.: Dynamics of sheared convective boundary layer entrainment. Part II: Evaluation of bulk model predictions of entrainment flux, *J. Atmos. Sci.*, 63, 1179–1199, doi:10.1175/JAS3696.1, 2006. 7203

Duynkerke, P. G.: Radiation fog: a comparison of model simulation with detailed observations, *Mon. Weather Rev.*, 119, 324–341, doi:10.1175/1520-0493(1991)119<0324:RFACOM>2.0.CO;2, 1991. 7217

Guenther, A., Karl, T., Harley, P., Wiedinmyer, C., Palmer, P. I., and Geron, C.: Estimates of global terrestrial isoprene emissions using MEGAN (Model of Emissions of Gases and Aerosols from Nature), *Atmos. Chem. Phys.*, 6, 3181–3210, doi:10.5194/acp-6-3181-2006, 2006. 7220, 7229

Janssen, R. H. H., Vilà-Guerau de Arellano, J., Ganzeveld, L. N., Kabat, P., Jimenez, J. L., Farmer, D. K., van Heerwaarden, C. C., and Mammarella, I.: Combined effects of surface conditions, boundary layer dynamics and chemistry on diurnal SOA evolution, *Atmos. Chem. Phys.*, 12, 6827–6843, doi:10.5194/acp-12-6827-2012, 2012. 7199, 7200

Janssen, R. H. H., Vilà-Guerau de Arellano, J., Jimenez, J. L., Ganzeveld, L. N., Robinson, N. H., Allan, J. D., Coe, H., and Pugh, T. A. M.: Influence of boundary layer dynamics and isoprene chemistry on the organic aerosol budget in a tropical forest, *J. Geophys. Res.-Atmos.*, 118, 9351–9366, doi:10.1002/jgrd.50672, 2013. 7199, 7201

Jarvis, P. G.: The interpretation of the variations in leaf water potential and stomatal conductance found in canopies in the field, *Philos. T. R. Soc. B*, 273, 593–610, doi:10.1098/rstb.1976.0035, 1976. 7215

Jöckel, P., Sander, R., Kerkweg, A., Tost, H., and Lelieveld, J.: Technical Note: The Modular Earth Submodel System (MESSy) – a new approach towards Earth System Modeling, *Atmos. Chem. Phys.*, 5, 433–444, doi:10.5194/acp-5-433-2005, 2005. 7229

Jöckel, P., Tost, H., Pozzer, A., Brühl, C., Buchholz, J., Ganzeveld, L., Hoor, P., Kerkweg, A., Lawrence, M. G., Sander, R., Steil, B., Stiller, G., Tanarhte, M., Taraborrelli, D., van Aardenne, J., and Lelieveld, J.: The atmospheric chemistry general circulation model ECHAM5/MESSy1: consistent simulation of ozone from the surface to the mesosphere, *Atmos. Chem. Phys.*, 6, 5067–5104, doi:10.5194/acp-6-5067-2006, 2006. 7198

Jöckel, P., Kerkweg, A., Buchholz-Dietsch, J., Tost, H., Sander, R., and Pozzer, A.: Technical Note: Coupling of chemical processes with the Modular Earth Submodel System (MESSy) submodel TRACER, *Atmos. Chem. Phys.*, 8, 1677–1687, doi:10.5194/acp-8-1677-2008, 2008. 7229

Boundary layer dynamics with MXL/MESSy

R. H. H. Janssen and
A. Pozzer

Title Page

Abstract

Introduction

Conclusions

References

Tables

Figures

⏪

⏩

◀

▶

Back

Close

Full Screen / Esc

Printer-friendly Version

Interactive Discussion



Pino, D., Vilà-Guerau de Arellano, J., and Duynkerke, P. G.: The contribution of shear to the evolution of a convective boundary layer, *J. Atmos. Sci.*, 60, 1913–1926, doi:10.1175/1520-0469(2003)060<1913:TCOSTT>2.0.CO;2, 2003. 7203

Pino, D., Vilà-Guerau de Arellano, J., and Kim, S.-W.: Representing sheared convective boundary layer by zeroth- and first-order-jump mixed-layer models: large-eddy simulation verification, *J. Appl. Meteorol. Clim.*, 45, 1224–1243, doi:10.1175/JAM2396.1, 2006. 7199, 7202

Pugh, T. A. M., MacKenzie, A. R., Hewitt, C. N., Langford, B., Edwards, P. M., Furneaux, K. L., Heard, D. E., Hopkins, J. R., Jones, C. E., Karunaharan, A., Lee, J., Mills, G., Misztal, P., Moller, S., Monks, P. S., and Whalley, L. K.: Simulating atmospheric composition over a South-East Asian tropical rainforest: performance of a chemistry box model, *Atmos. Chem. Phys.*, 10, 279–298, doi:10.5194/acp-10-279-2010, 2010. 7209

Pugh, T. A. M., MacKenzie, A. R., Langford, B., Nemitz, E., Misztal, P. K., and Hewitt, C. N.: The influence of small-scale variations in isoprene concentrations on atmospheric chemistry over a tropical rainforest, *Atmos. Chem. Phys.*, 11, 4121–4134, doi:10.5194/acp-11-4121-2011, 2011. 7209

Sander, R., Baumgaertner, A., Gromov, S., Harder, H., Jöckel, P., Kerkweg, A., Kubistin, D., Regelin, E., Riede, H., Sandu, A., Taraborrelli, D., Tost, H., and Xie, Z.-Q.: The atmospheric chemistry box model CAABA/MECCA-3.0, *Geosci. Model Dev.*, 4, 373–380, doi:10.5194/gmd-4-373-2011, 2011. 7198, 7219, 7229

Sander, R., Jöckel, P., Kirner, O., Kunert, A. T., Landgraf, J., and Pozzer, A.: The photolysis module JVAL-13.99gmdd, compatible with the MESSy standard, and the JVal PreProcessor (JVPP), *Geosci. Model Dev. Discuss.*, 7, 2501–2523, doi:10.5194/gmdd-7-2501-2014, 2014. 7220, 7229

Taraborrelli, D., Lawrence, M. G., Butler, T. M., Sander, R., and Lelieveld, J.: Mainz Isoprene Mechanism 2 (MIM2): an isoprene oxidation mechanism for regional and global atmospheric modelling, *Atmos. Chem. Phys.*, 9, 2751–2777, doi:10.5194/acp-9-2751-2009, 2009. 7221

Tennekes, H.: A model for the dynamics of the inversion above a convective boundary layer, *J. Atmos. Sci.*, 30, 558–567, doi:10.1175/1520-0469(1973)030<0558:AMFTDO>2.0.CO;2, 1973. 7199, 7200, 7202

Tennekes, H. and Driedonks, A.: Basic entrainment equations for the atmospheric boundary layer, *Bound.-Lay. Meteorol.*, 20, 515–531, doi:10.1007/BF00122299, 1981. 7203

**Boundary layer
dynamics with
MXL/MESSy**R. H. H. Janssen and
A. Pozzer

Title Page

Abstract

Introduction

Conclusions

References

Tables

Figures

◀

▶

◀

▶

Back

Close

Full Screen / Esc

Printer-friendly Version

Interactive Discussion



- Tsimpidi, A. P., Karydis, V. A., Pozzer, A., Pandis, S. N., and Lelieveld, J.: ORACLE: a module for the description of ORganic Aerosol Composition and Evolution in the atmosphere, *Geosci. Model Dev. Discuss.*, 7, 5465–5515, doi:10.5194/gmdd-7-5465-2014, 2014. 7220, 7229
- 5 Van Heerwaarden, C. C.: Surface Evaporation and Water Vapor Transport in the Convective Boundary Layer, Ph.D. thesis, Wageningen University, Wageningen, the Netherlands, 2011. 7212
- Van Heerwaarden, C. C., Vilà-Guerau de Arellano, J., Moene, A. F., and Holtslag, A. A. M.: Interactions between dry-air entrainment, surface evaporation and convective boundary-layer development, *Q. J. Roy. Meteor. Soc.*, 135, 1277–1291, doi:10.1002/qj.431, 2009. 7200, 7212
- 10 Van Heerwaarden, C. C., Vilà-Guerau de Arellano, J., Gounou, A., Guichard, F., and Couvreux, F.: Understanding the daily cycle of evapotranspiration: a method to quantify the influence of forcings and feedbacks, *J. Hydrometeorol.*, 11, 1405–1422, doi:10.1175/2010JHM1272.1, 2010. 7200, 7212
- 15 van Stratum, B. J. H., Vilà-Guerau de Arellano, J., Ouwersloot, H. G., van den Dries, K., van Laar, T. W., Martinez, M., Lelieveld, J., Diesch, J.-M., Drewnick, F., Fischer, H., Hosaynali Beygi, Z., Harder, H., Regelin, E., Sinha, V., Adame, J. A., Sörgel, M., Sander, R., Bozem, H., Song, W., Williams, J., and Yassaa, N.: Case study of the diurnal variability of chemically active species with respect to boundary layer dynamics during DOMINO, *Atmos. Chem. Phys.*, 12, 5329–5341, doi:10.5194/acp-12-5329-2012, 2012. 7199, 7220, 7221, 7231
- Vilà-Guerau de Arellano, J., van den Dries, K., and Pino, D.: On inferring isoprene emission surface flux from atmospheric boundary layer concentration measurements, *Atmos. Chem. Phys.*, 9, 3629–3640, doi:10.5194/acp-9-3629-2009, 2009. 7199, 7200, 7209
- 25 Vilà-Guerau de Arellano, J., Patton, E. G., Karl, T., van den Dries, K., Barth, M. C., and Orlando, J. J.: The role of boundary layer dynamics on the diurnal evolution of isoprene and the hydroxyl radical over tropical forests, *J. Geophys. Res.*, 116, D07304, doi:10.1029/2010JD014857, 2011. 7199, 7209
- Vilà-Guerau de Arellano, J., van Heerwaarden, C. C., and Lelieveld, J.: Modelled suppression of boundary-layer clouds by plants in a CO₂-rich atmosphere, *Nat. Geosci.*, 5, 701–704, doi:10.1038/ngeo1554, 2012. 7200
- 30

Vilà-Guerau de Arellano, J., van Heerwaarden, C., van Stratum, B., and van den Dries, K.: Atmospheric Boundary Layer: Integrating Chemistry and Land Interactions, Cambridge University Press, Cambridge, UK, in press, 2015. 7200, 7218

5 Vinuesa, J.-F. and Vilà-Guerau de Arellano, J.: Fluxes and (co-)variances of reacting scalars in the convective boundary layer, Tellus B, 55, 935–949, doi:10.1046/j.1435-6935.2003.00073.x, 2003. 7209

GMDD

7, 7197–7238, 2014

Boundary layer dynamics with MXL/MESSy

R. H. H. Janssen and
A. Pozzer

Title Page

Abstract

Introduction

Conclusions

References

Tables

Figures



Back

Close

Full Screen / Esc

Printer-friendly Version

Interactive Discussion



Boundary layer dynamics with MXL/MESSy

R. H. H. Janssen and
A. Pozzer

Title Page

Abstract

Introduction

Conclusions

References

Tables

Figures

◀

▶

◀

▶

Back

Close

Full Screen / Esc

Printer-friendly Version

Interactive Discussion



Table A2. Initial mixing ratio in ABL and FT, and surface emission fluxes of the reactants for the different runs in MXL/MESSy and MXLCH. Species in the reaction mechanism that are not included in this table have zero initial concentrations and zero surface emissions. For O₂ and N₂ we have imposed the values 2×10^8 and 8×10^8 ppb, respectively.

	O ₃	NO	NO ₂	ISO	CH ₄	CO	H ₂ O ₂
Van Stratum et al. (2012)							
Initial mixing ratio (ppb)							
ABL	30.0	0.0	0.6	0.0	1724.0	105.0	0.1
FT	39.0	0.0	0.0	0.0	1724.0	105.0	0.1
Surface emission flux (mg m ⁻² h ⁻¹)	0.0	0.13	0.0	$0.30 \sin\left(\frac{\pi t}{t_d}\right)$	0.0	0.0	0.0
BestFit MXL/MESSy							
Initial mixing ratio (ppb)							
ABL	30.0	0.008	0.65	0.0	1742.0	105.0	0.1
FT	41.0	0.0	0.0	0.0	1742.0	105.0	0.1
Surface emission flux (mg m ⁻² h ⁻¹)	0.0	0.07	0.0	$0.15 \sin\left(\frac{\pi t}{t_d}\right)$	0.0	0.0	0.0

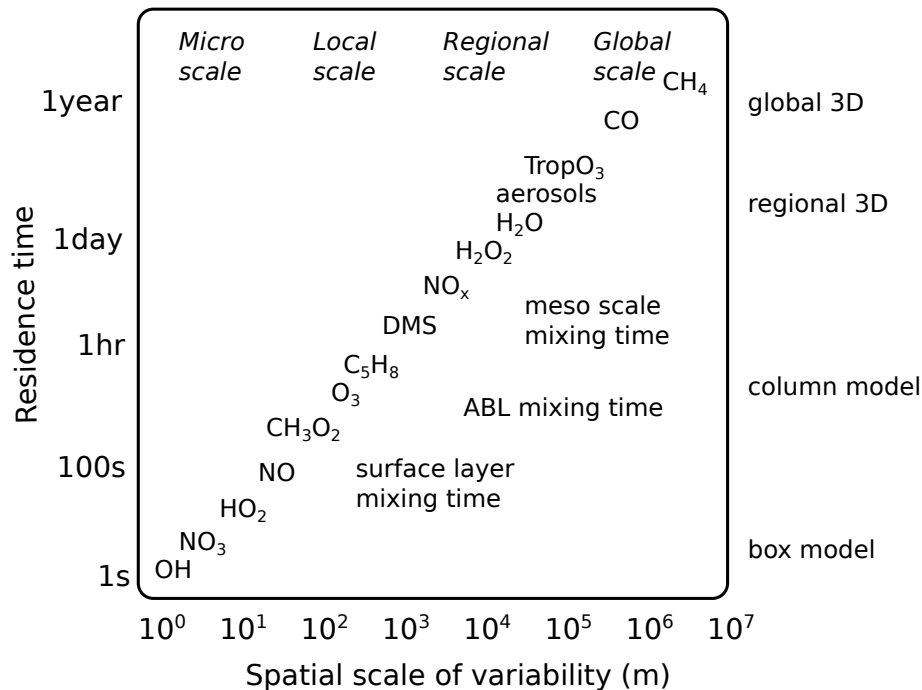


Figure 1. Spatio-temporal scales in atmospheric chemistry, typical species associated with these scales and the type of model that should be used to study their behaviour in the atmosphere.

Boundary layer dynamics with MXL/MESSy

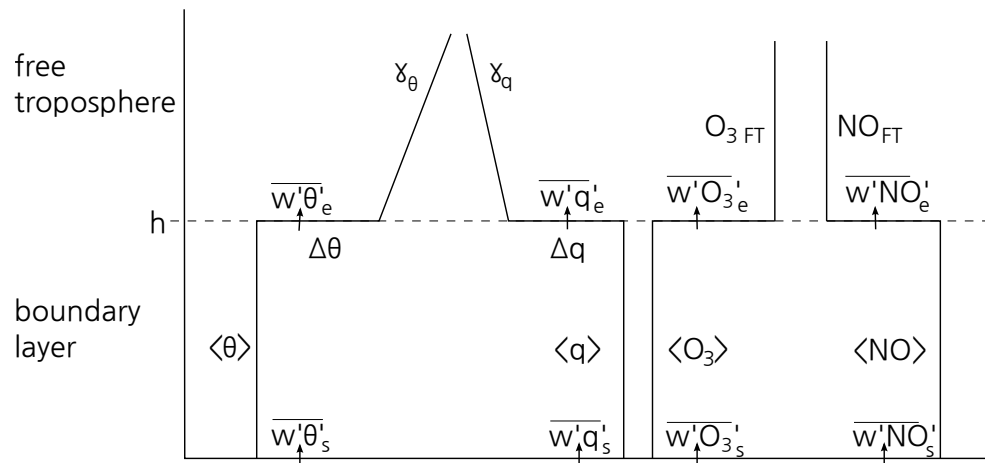
R. H. H. Janssen and
A. Pozzer

Figure 2. Typical mixed-layer profiles of potential temperature (θ), specific humidity (q) and chemical species (in this case O_3 and NO). Also surface and entrainment fluxes of heat, moisture, O_3 and NO are indicated; the arrows indicate the direction in which the flux is defined positively.

Title Page

Abstract

Introduction

Conclusions

References

Tables

Figures

◀

▶

◀

▶

Back

Close

Full Screen / Esc

Printer-friendly Version

Interactive Discussion



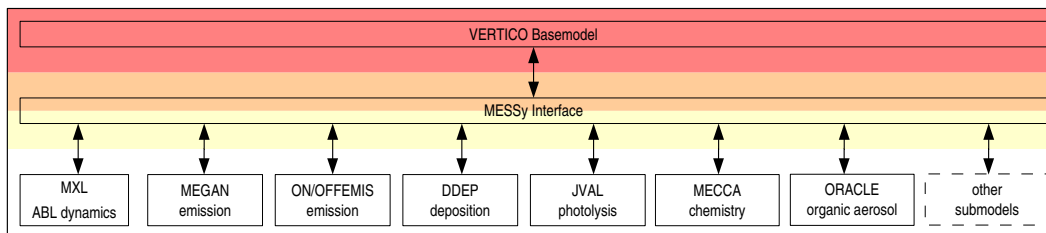
**Boundary layer dynamics with
MXL/MESSy**R. H. H. Janssen and
A. Pozzer

Figure 3. Scheme of the implementation of the VERTICO basemodel in the MESSy structure and the coupling to the MXL and other submodels through the MESSy interface.

[Title Page](#)[Abstract](#)[Introduction](#)[Conclusions](#)[References](#)[Tables](#)[Figures](#)[◀](#)[▶](#)[◀](#)[▶](#)[Back](#)[Close](#)[Full Screen / Esc](#)[Printer-friendly Version](#)[Interactive Discussion](#)

Boundary layer dynamics with MXL/MESSy

R. H. H. Janssen and
A. Pozzer

Title Page

Abstract

Introduction

Conclusions

References

Tables

Figures

◀

▶

◀

▶

Back

Close

Full Screen / Esc

Printer-friendly Version

Interactive Discussion

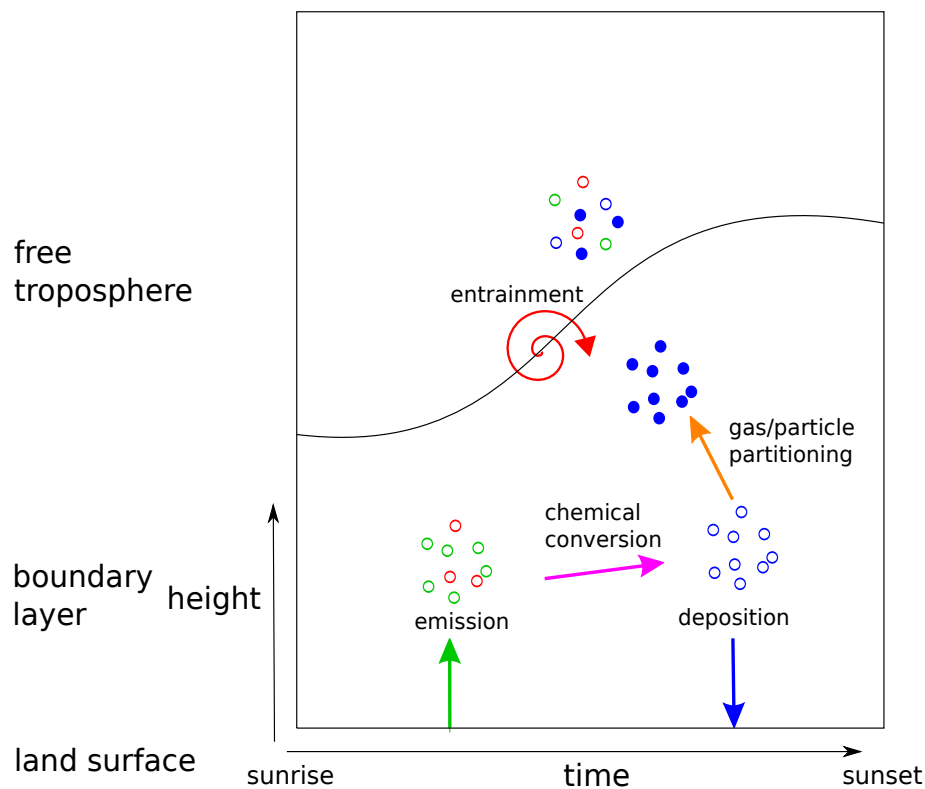


Figure 4. Processes relevant to evolution of species concentrations in the boundary layer. Open and closed circles depict gas-phase and aerosol-phase species, respectively.

Boundary layer dynamics with MXL/MESSy

R. H. H. Janssen and
A. Pozzer

Title Page

Abstract

Introduction

Conclusions

References

Tables

Figures

◀

▶

◀

▶

Back

Close

Full Screen / Esc

Printer-friendly Version

Interactive Discussion

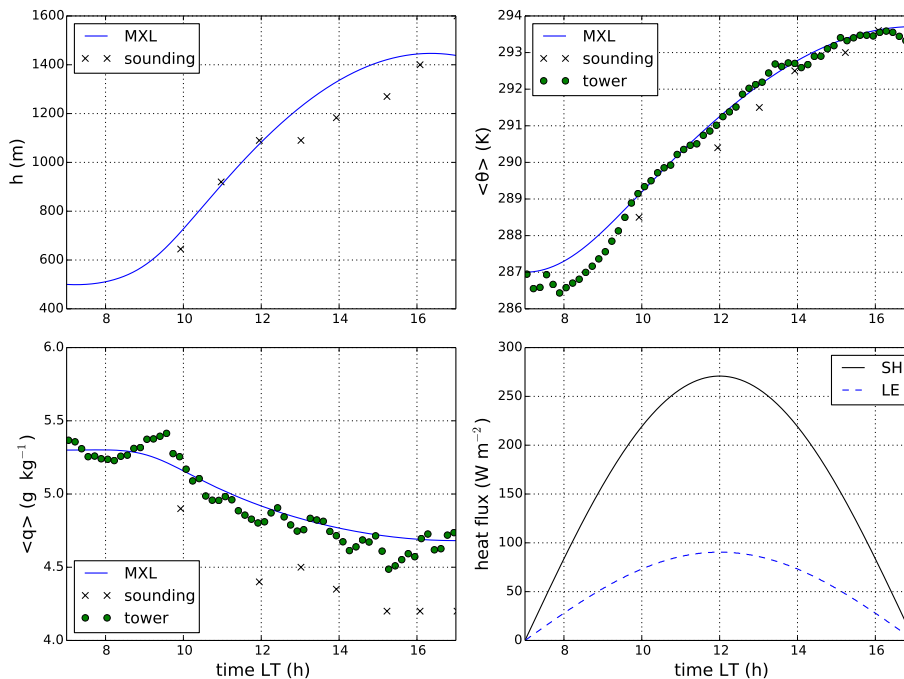


Figure 5. Diurnal evolution of observed and modelled **(a)** mixed-layer height (h), **(b)** mixed-layer potential temperature (θ), **(c)** mixed-layer specific humidity (q) and **(d)** prescribed sensible (SH) and latent (LE) heat fluxes.

Boundary layer dynamics with MXL/MESSy

R. H. H. Janssen and A. Pozzer

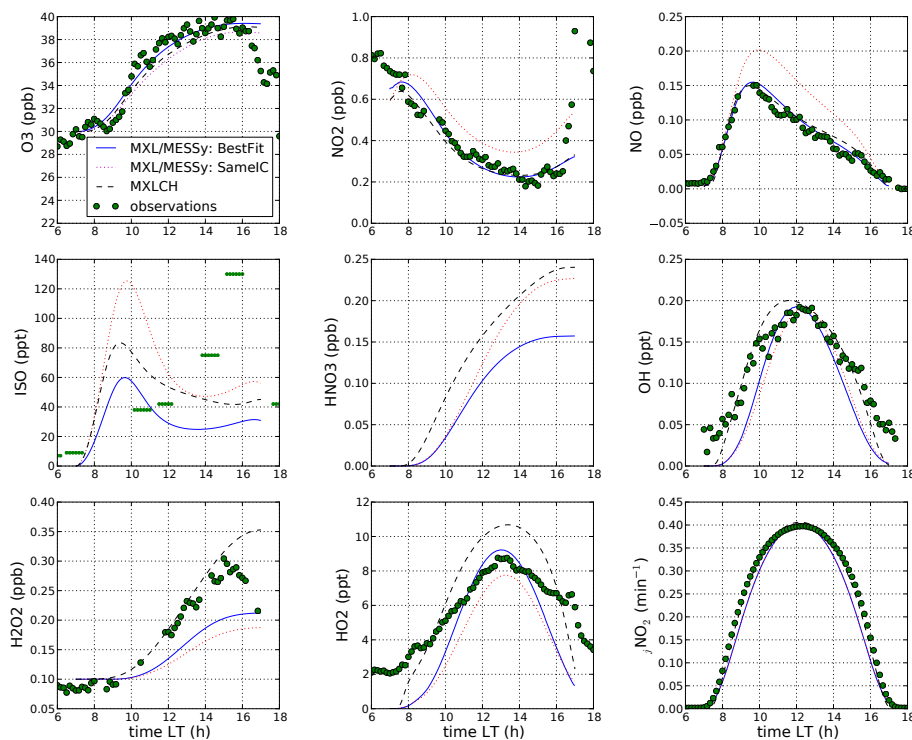


Figure 6. Observed and modelled diurnal evolution of gas-phase chemistry and NO_2 photolysis rate for the DOMINO case, comparing MXL/MESSy and MIM2 chemistry with MXLCH and reduced chemistry. Results for both the SameIC and the BestFit runs with MXL/MESSy are shown.

Title Page

Abstract

Introduction

Conclusions

References

Tables

Figures

◀

▶

◀

▶

Back

Close

Full Screen / Esc

Printer-friendly Version

Interactive Discussion



Boundary layer dynamics with MXL/MESSy

R. H. H. Janssen and A. Pozzer

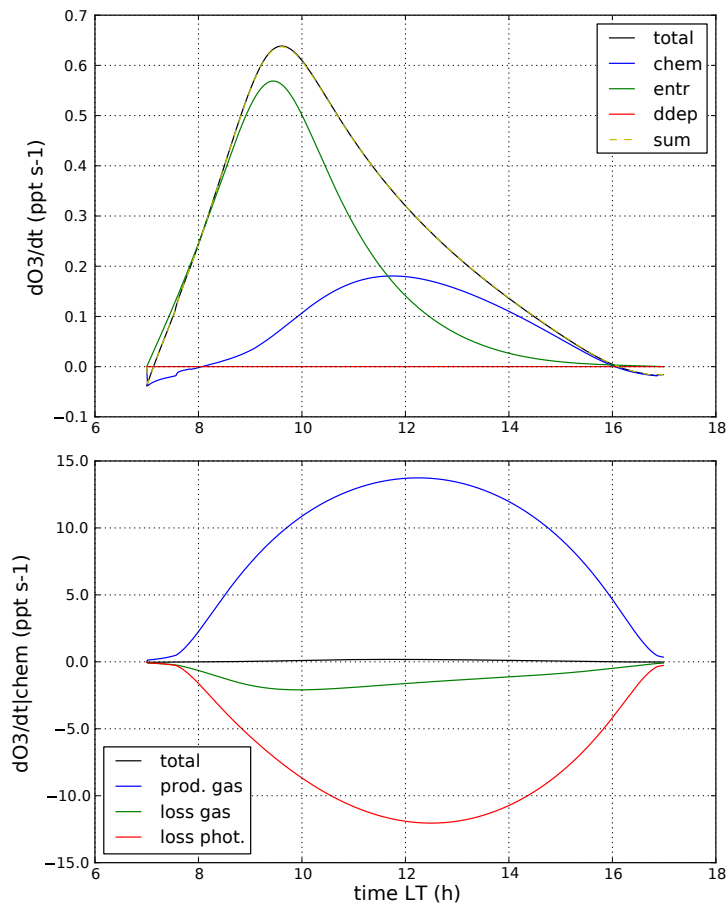


Figure 7. O_3 budget for the DOMINO case showing the contributions of (a) the processes entrainment, chemistry and dry deposition and (b) the chemical production and loss with the chemical loss split up in a gas-phase destruction and a photolysis term.